Modeling Future Land Cover Changes and Their Effects on the Land Surface Temperatures in the Saudi Arabian Eastern Coastal City of Dammam

Muhammad Tauhidur Rahman [1,*], Adel S. Aldosary [1] and Md. Golam Mortoja [2]

[1] Department of City and Regional Planning, King Fahd University of Petroleum and Minerals, KFUPM Box 5053, Dhahran 31261, Saudi Arabia; asdosary@kfupm.edu.sa
[2] ICT-GIS Division, Institute of Water Modelling, House #496, Road # 32, New DOHS, Mohakhali, Dhaka 1206, Bangladesh; himu3107@gmail.com
* Correspondence: mtr@kfupm.edu.sa; Tel.: +966-13-860-7364

Abstract: Over the past several decades, Saudi cities have experienced rapid urban developments and land use and land cover (LULC) changes. These developments will have numerous short- and long-term consequences including increasing the land surface temperature (LST) of these cities. This study investigated the effects of LULC changes on the LST for the eastern coastal city of Dammam. Using Landsat imagery, the study first detected the LULC using the maximum likelihood classification method and derived the LSTs for the years 1990, 2002, and 2014. Using the classified results, it then modeled the future LULC for 2026 using the Cellular Automata Markov (CAM) model. Finally, using three thematic indices and linear regression analysis, it then modeled the LST for 2026 as well. The built-up area in Dammam increased by 28.9% between 1990 and 2014. During this period, the average LSTs for the LULC classes increased as well, with bare soil and built-up area having the highest LST. By 2026, the urban area is expected to encompass 55% of the city and 98% of the land cover is envisioned to have average LSTs over 41 °C. Such high temperatures will make it difficult for the residents to live in the area.

1. Introduction

Every year, human migrations to cities are causing urban areas to grow and bringing rapid changes to their ecosystem, biodiversity, natural landscapes, and the environment [1,2]. While such growth is a sign of the region's employment growth and economic prosperity, it has numerous short- and long-term consequences. Among the long-term consequences, increases in the city's land surface temperature (LST) from growing urban built-up areas have received wide attention from geographers, urban planners, and climatologists over the past decade [3,4]. Studies show that urban expansion tends to increase urban areas' LSTs by an average of 2–4 °C when compared to their outskirt rural areas [5]. Rising LSTs and urban heat island (UHI) formations have been linked to high energy consumption, air pollution, and human health problems including asthma and heat-stroke related deaths of children and elders [6,7].

Over the past several decades, cities in the Kingdom of Saudi Arabia have been rapidly expanding from economic prosperity and increasing migrating population from villages and working expatriates from neighboring Asian countries [8]. In 1950, only 21% of the Kingdom's residents lived in a major city [9]. That number increased to 58% in 1975, and today, urban areas house 82% of the country's

population, with many of the urban residents having migrated to the cities in an effort to seek a modern lifestyle, better employment, and/or educational opportunities [9,10]. To fulfill the needs of the settling residents, multi-story apartment buildings and private villas along with commercial and industrial facilities were built, and areas that were small villages in the 1940s transformed into present day major cities and metropolitan areas. The eastern coastal city of Dammam is one such city; it was a small fishing village in the 1940s that rapidly expanded in the last three decades due to the booming of oil industries and became a major metropolitan city (with its neighboring cities of Dhahran and Khobar) and the capitol of the Eastern Province of Saudi Arabia [11]. Such expansions significantly changed the land use and land cover (LULC) and are expected to affect and increase the city's LSTs.

Examining LULC changes has become an increasing concern throughout the recent decades because of their roles in reducing biodiversity, modifying the ecosystem, and altering the pattern and composition of the regional and global climate [12]. Detecting and monitoring LULC changes through direct field visits can be difficult, time consuming, and are prone to producing inaccurate results. Improvements and integration of remote sensing and Geographic Information Systems (GIS) in the past several decades have resolved some of these limitations and today are powerful tools for assessing, monitoring, and modelling LULC changes [13–16]. They have been utilized to examine LULC changes in Saudi cities as well. Using Landsat TM data, Alwashe and Bokhari [17] studied the changes in vegetation in the city of Al Madinah. Also using Landsat TM data, Al-Rowili et al. [18] monitored and identified decadal urban areal changes in Jeddah between 1988 and 1998. Aljoufie et al. [19] tried to assess the relationships between transportation systems and urban expansion for Jeddah by aerial photographs, SPOT imagery, and the city's Master plan. For the city of Tabuk, Al-Harbi [20] measured agricultural land use changes based on Landsat TM and Spot 5 imagery collected from 1988 to 2008. Al-Gaadi et al. [21] monitored changes from 1990 to 2006 of Dirab region from Landsat data. Finally, Rahman [8] also used Landsat TM, ETM+, and OLI data to examine growth in Al-Khobar from 1990 and 2013.

Since the early 1970s, the application of remote sensing technologies for measuring LSTs and examining the formation and spatial distribution of UHIs has also been quite promising [22]. Using the various available thermal infrared sensors that can collect data at various spatial resolutions, researchers have studied the LST characteristics (per LULC categories) in different urban settings. Using Landsat TM data collected over Twin Cities, Minnesota, Yuan and Bauer [23] studied the relationships among LSTs, normalized difference vegetation index (NDVI), and percentage of impervious surface area (ISA). Xiao et al. [24] measured LSTs from Landsat TM sensor and determined their quantitative relationships with several biophysical and demographic variables for Beijing city. Also in Beijing, Li et al. [25] observed the correlations between the spatio-temporal trends in LSTs obtained from Landsat TM sensor and the configuration of greenspaces (classified from SPOT imagery). By collecting LSTs retrieved from the AVHRR sensor and combining it with land coverage classified from SPOT-HRV data, Dousset and Gourmelon [26] studied the relationships between different land covers and LSTs in the metropolises of Los Angeles and Paris. Recently, Chaudhuri and Mishra [27] compared the LSTs (from Landsat data) among the various types of land coverage in the border cities of Calcutta (India) and Khulna (Bangladesh). Also for Bangladesh, Ahmed et al. [28] first measured the LSTs and the decadal LULC changes in Dhaka metropolitan area from Landsat sensors. They then modelled the growth of the city and simulated the LSTs of the built-up areas for 2029. Among the Middle Eastern cities, El Abidine et al. [29] modelled the heat waves by examining the relationships between LST and the variations among the LULC categories in the entire state of Qatar. A similar study was also conducted by Rasul et al. [30] using Landsat 8 data to compare LSTs in different LULC categories in the northern Kurdistan Iraqi city of Erbil. Lazzarini et al. [31] combined MODIS, ASTER, and Landsat ETM+ data and found the association between LST, NDVI, and surface UHI at the city and district level for the city of Abu Dhabi, United Arab Emirates. For the Kingdom of Bahrain, Radhi and Sharples [32] used a combination of Landsat imagery, statistics, and weather station data to examine urban developments and their impacts in forming UHIs during the last few decades.

Based on a review of the literature, it was found that examining the LULC changes and their impacts on the LSTs is lacking in Saudi Arabia's Eastern Province in general and particularly in its capital city of Dammam. This study aims to fill that gap. Specifically, we first examined the LULC changes within Dammam over the past two decades (1990–2014) using recent and historical archived Landsat satellite data. Using the Landsat's thermal infrared sensor, we then investigated the changes in the LSTs for each LULC category during these two decades. Finally, based on the city's historical development, we modelled future growth of Dammam and its corresponding changes in LSTs for the year 2026. In Sections 2 and 3, the study area's description along with the detailed methodology will be presented. Section 4 will highlight the results and their discussions will be provided in Section 5. Finally, the concluding remarks and paths for further research are presented in Section 6.

2. Study Area

The entire city of Dammam (26.32° N and 49.50° E) with an area of 653 km^2 was the area under consideration for this study (Figure 1). Dammam currently has an estimated population of 1,106,630. Almost 58% of the residents are Saudis with the rest migrating from the neighboring Middle Eastern, Asian, and Western countries [33]. Having a desert climate, the summers are hot and humid (temperatures varying from 30 °C–45 °C) while the winters are cool and dry (10 °C–21 °C) [34].
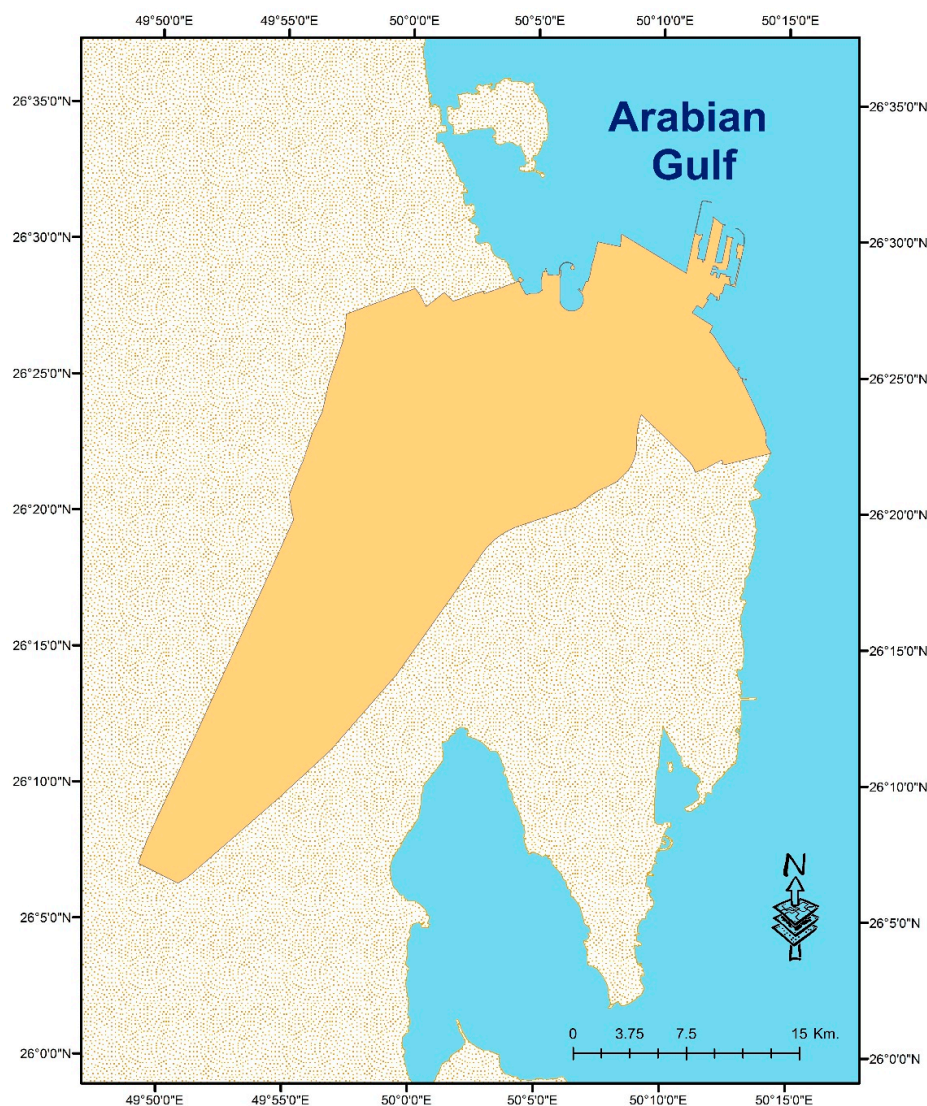
Figure 1. Study area in the eastern coast of Saudi Arabia.

3. Methodology

3.1. Data Collection, Classification, Accuracy Assessments

Three Landsat images processed at level-one terrain-corrected (L1T) level collected over the city of Dammam from the years 1990, 2002, and 2014 were gathered from the United States Geological Survey's (USGS) EarthExplorer website to estimate the LULC changes and calculate the LSTs for the respective years (Table 1). Since L1T data are delivered with corrected radiometric and geometric distortions, no additional geo-rectification or image-to-image registrations were performed. Also, USGS resampled and provided all the Landsat thermal bands to 30 m to align with the multispectral bands of the sensors [35]. Finally, a recent high resolution GeoEye image was acquired for classification and accuracy assessments.

Table 1. Characteristics of Landsat data sets for the study.

Date of Acquisition	Path and Row	Landsat Sensor	Spatial Resolution of Multi-Spectral Bands	Spatial Resolution of Thermal Bands
16 August 1990	164/42	TM	30 m	120 m (resampled to 30 m)
24 July 2002	164/42	ETM+	30 m	60 m (resampled to 30 m)
2 August 2014	164/42	OLI	30 m	100 m (resampled to 30 m)

The imagery was classified into four separate LULC classes based on Level 1 of the Anderson Classification scheme. It is the preferred classification system for classifying Landsat data [36]. Table 2 highlights the LULC features included for each class. To classify the LULC from the three pre-processed Landsat images, the Maximum Likelihood Classification (MLC) technique was used with signatures collected among the four classes identified through field surveys, GeoEye image, and Google Earth imagery.

Table 2. Scheme for land cover classifications.

Land Cover Class	Description
Built-up	Residential, industrial, transportation networks, and commercial infrastructures.
Bare soil	Sand, vacant lands, bare soils.
Vegetation	Trees, parks, playgrounds, grasslands.
Water body	Lakes and coastal water.

To examine the classification accuracies, 295 ground truth reference points were sampled (through stratified random sampling method) across the study area. Historical LULC paper maps (with scales of 1:32,258) were also collected from the Ad-Dammam municipality's office. These historical maps, ground truth reference points, and high resolution GeoEye and Google Earth images were all utilized in combination to measure the overall classification accuracies. For comparison of accuracy results, error matrices were created. The classified results had overall accuracies of 86% (1990), 89% (2002), and 93% (2014) with Kappa coefficients of 0.87, 0.90, and 0.94. Finally, the changes between the classified data sets were examined using a post-classification change detection method.

3.2. Derivation of LSTs

The LSTs for this study were obtained from Landsat's thermal band(s). Landsat TM and ETM+ provide thermal information based on a single long-wave infrared (LWIR) band, whereas it is captured with two LWIR bands by the Landsat OLI sensor [37]. Therefore, two separate methods were used to derive the LSTs from the three sensors. For deriving the LSTs from Landsat TM and ETM+ sensors,

the Spectral Radiance Scaling Method was used [38]. The method first uses the following equation to convert digital numbers (*DNs*) into spectral radiance (L_λ):

$$L_\lambda = \frac{(LMAX_\lambda - LMIN_\lambda) \times (DN - QCALMIN)}{QCALMAX - QCALMIN} + LMIN_\lambda \tag{1}$$

where *DN* values range between 0 and 255; $LMIN_\lambda$ and $LMAX_\lambda$ are the minimum and maximum spectral radiances, respectively; and *QCALMIN* and *QCALMAX* are quantized minimum and maximum calibrated pixel values, respectively.

The second step involved utilizing Equation (2) to convert the spectral radiance to Brightness Temperature (in Kelvin) [39,40]. Temperatures were then converted to degrees Celsius.

$$T_K = \frac{K_2}{\ln(\frac{K_1}{L_\lambda} + 1)} \tag{2}$$

To derive the LSTs for the year 2014 from the Landsat OLI data, Equations (3) and (4) were used [41]:

$$TOA_r = mx + b \tag{3}$$

where TOA_r is the top of atmospheric radiance; *m* is the radiance multiplier (0.0003342); *x* is the raw band; and *b* is the radiance add (0.1) [42].

$$T_K = \frac{K_2}{\ln(\frac{K_1}{TOA_r} + 1)} \tag{4}$$

where T_K is the Temperature in degrees Kelvin; K_1 = 774.89 and K_2 = 1321.08. Temperatures were converted to degrees Celsius as well.

3.3. Modeling the Land Cover for 2026

Numerous urban growth prediction models (UGPMs) are available for modelling the future land use and land cover of an urban area [43]. In this study, modelling the LULC for the year 2026 was completed using IDRISI Selva GIS software package. To choose the most accurate modeling technique for forecasting the LULC of Dammam for 2026, we simulated the LULC of Dammam for 2014 using three separate but popular LULC modeling methods (Cellular Automata Markov (CAM), Multi-Layer Perception Markov (MLPM), and Stochastic Markov (SM)) and examined their accuracies. In all of the three models, the LULC for 2014 was simulated using the classification results from 1990 (earlier land cover) and 2002 (later land cover).

To model using the CAM method, a combination of Cellular Automata (CA) with Markov Chain Analysis was utilized. It first involved using the classified LULC data from 1990 and 2002 to produce the Markovian conditional probability areas. Then, Boolean images for each LULC type were generated using the 2002 classified results. Euclidean distances for each Boolean image were then calculated and suitability images using "FUZZY Factor Standardization" were generated. Finally, the CAM method utilized the Markovian conditional probability areas and suitability images to generate the LULC model for 2014. The CAM modeling technique has successfully modelled future LULC changes in several major cities in the world [44–47].

The MLPM modelling method utilizes and combines the concepts of Artificial Neural Network (ANN) and Markov Chain Analysis (MCA). To model, it first calculated the changes in the LULC between 1990 and 2002 and selected the driver variables (distance from bare soil; distance from vegetation; distance form water body; distance from built-up area; and empirical likelihood) to predict the transitions or changes. The strength of each variable was measured using Cramer's Value. The transition sub-model was created and modified until a maximum accuracy of 82.05% was achieved. The models showed that the LULC exhibited three potential transitional forms: bare soil to built-up

areas, vegetation to built-up areas, and built-up areas to bare soil. It should be highlighted that conversion of built-up areas to bare soil/sand is usually rare. However, the study area experiences frequent sand-storms and strong winds and roads and highways are frequently found covered with sands due to these natural meteorological phenomena. It is possible for these areas to be classified as built-up areas in one year (when sands are not present) but as soil/sand at a later year when sands cover them. Hence conversion of built-up area to bare soil was found to be a valid potential transitional form. The transition potential map for each transition was produced and the LULCs for 2014 were modeled. Previous studies have found MLPM to produce better prediction accuracies in areas featuring stable and slow LULC changes [48]. Finally, in the SM model, Markovian conditional probability images from the years 1990 to 2002 were produced using the Markov module of IDRISI. The Stochastic choice was then applied to materialize the conditional probability images generated from Markov analysis.

Once the LULCs for 2014 were modeled using the three methods, the Map Comparison Kit (MCK) software was utilized to find the best-fit model. To select the best-fit model, the overall Kappa, Khisto, Klocation, and Fraction correct was calculated and examined [49]. The calculated results are shown in Table 3. Since the CAM model had the highest overall Kappa coefficients and Fraction correct, it was used to simulate the LULC for 2026.

Table 3. Comparison of overall Kappa statistics for three modeling results for 2014.

Kappa Components	CAM	SM	MLPM
Overall Kappa	0.56	0.30	0.45
Overall Klocation	0.67	0.36	0.62
Overall Khisto	0.83	0.83	0.73
Fraction Correct	0.75	0.60	0.69

3.4. Modeling of LST for 2026

After simulating the LULC for 2026, this study modified the methodology proposed by [28] to model and map the distribution of the LSTs across Dammam city. First, several land cover indices of each LULC type for the years 1990, 2002, and 2014 were derived. The indices were the Normalized Difference Bare Soil Index (NDBsI), NDVI, Soil Adjustment Vegetation Index (SAVI), Normalized Difference Water Body Index (NDWI), Modified Normalized Difference Water Body Index (MNDWI), and Normalized Difference Built-up Area Index (NDBI). The equations used to calculate the indices along with their references are given in Table 4.

Table 4. Indices used to model land surface temperature (LST) for 2026.

Index	Equation		Reference
	Landsat TM and ETM+	Landsat OLI	
NDBsI	$\frac{B5 - B6}{B5 + B6}$	$\frac{B6 - B10}{B6 + B10}$	[50]
NDVI	$\frac{B4 - B3}{B4 + B3}$	$\frac{B5 - B4}{B5 + B4}$	[50]
SAVI	$\frac{1.5\,(B4 - B3)}{B4 + B3 + 0.5}$	$\frac{1.5\,(B5 - B4)}{B5 + B4 + 0.5}$	[51]
NDWI	$\frac{B2 - B4}{B2 + B4}$	$\frac{B3 - B5}{B3 + B5}$	[52]
MNDWI	$\frac{B2 - B5}{B2 + B5}$	$\frac{B3 - B6}{B3 + B6}$	[53]
NDBI	$\frac{B5 - B4}{B5 + B4}$	$\frac{B6 - B5}{B6 + B5}$	[54]

Once the indices were derived, simple linear regression analysis was performed to examine their relations with LSTs to select the indices that contribute the most for LST modeling. In the regression analysis, indices were the independent variables and LST was the dependent variable. The NDBI,

NDBsI, and MNDWI were found to be the major significant indices ($p < 0.05$) contributing to LSTs. The three indices were normalized on a scale of 0 to 1 and reclassified into 20 equal classes to fit for the usage of "Markov Chain Analysis". We then conducted "Markov Chain Analysis" and combined Stochastic Choice with Markov Chain Analysis to simulate the selected indices for the year 2026. Using the three normalized indices data and the *LST* for 2014, the following equation (with $r^2 = 0.729$) was formulated to explain their relationships:

$$LST = 81.81 - (17.92 \times NDBsI) - (4.79 \times NDBI) - (60.39 \times MNDWI) \tag{5}$$

where *NDBsI*, *NDBI*, and *MNDWI* are the corresponding indices and *LST* is the land surface temperature. Finally, the equation and simulated 2026 indices were used to model and map the *LST* for 2026.

4. Results

4.1. Changes in LULC in Dammam

The classified LULC results for the years 1990, 2002, and 2014 are given in Figure 2 while Table 5 shows their areal statistics, and changes among classes between the years are provided in Tables 6 and 7. From 1990 to 2014, the amount of bare soil declined significantly (by 16,632 ha or 25.5%). During the same period, the built-up area increased by 18,899 ha (28.9% of the study area). The amount of vegetation declined from the years 1990 to 2002 (by 1415 ha or 2.16% of the study area). However, an increase in vegetation was observed between 2002 and 2014 (by 671 ha or 1% of the study area). Finally, the areas of water slightly increased by 380 ha (0.6% of the study area) between 1990 and 2002 and decreased by 1903 ha (3% of the study area) from 2002 to 2014.

Table 5. Areal statistics (in hectares) of classified land cover for 1990, 2002, and 2014.

Land Cover Class	1990		2002		2014	
	Area	%	Area	%	Area	%
Bare soil/sand	48,863	74.79	44,227	67.69	32,231	49.33
Built-up area	9368	14.34	15,039	23.02	28,267	43.27
Vegetation	1785	2.73	370	0.57	1041	1.59
Water body	5317	8.14	5697	8.72	3794	5.81
Total	65,333	100	65,333	100	65,333	100

Table 6. Change detection matrix showing the class changes (in hectares) between 1990 and 2002.

		2002				
		Bare Soil/Sand	Built-Up Area	Vegetation	Water Body	Total
1990	Bare soil/sand	42,803	5969	74	17	48,863
	Built-up area	883	8061	37	387	9368
	Vegetation	438	949	252	146	1785
	Water body	103	60	7	5147	5317
	Total	44,227	15,039	370	5697	65,333

Table 7. Change detection matrix showing the class changes (in hectares) between 2002 and 2014.

		2014				
		Bare Soil/Sand	Built-Up Area	Vegetation	Water Body	Total
2002	Bare soil/sand	30,131	13,824	250	22	44,227
	Built-up area	995	13,427	608	9	15,039
	Vegetation	49	147	174	0	370
	Water body	1056	869	9	3763	5697
	Total	32,231	28,267	1041	3794	65,333
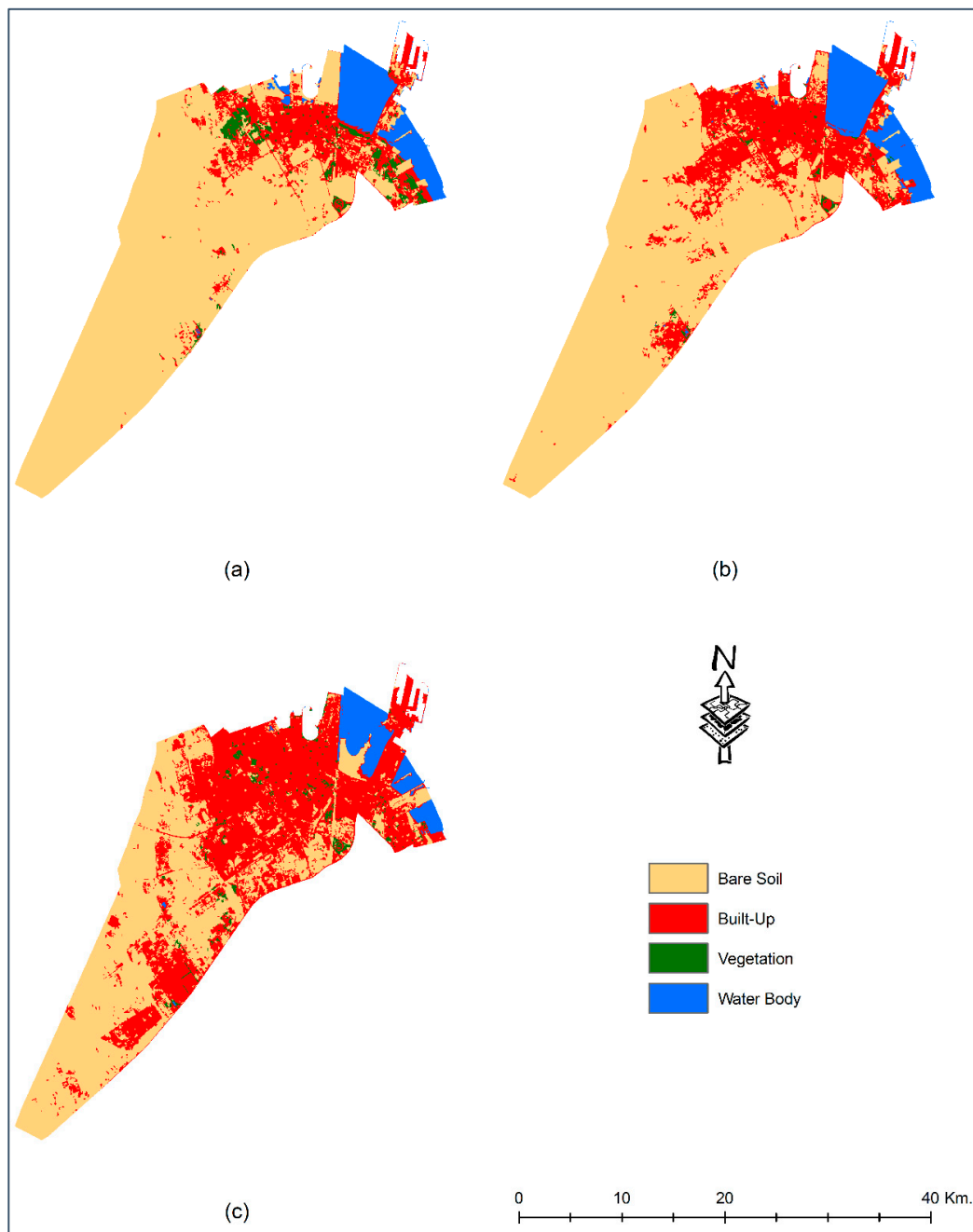
Figure 2. The study area's classification results for (**a**) 1990, (**b**) 2002, and (**c**) 2014.

*4.2. Distribution and Changes of LST in LULC in Dammam*

The average LSTs of individual LULC classes are provided in Table 8. It was observed that for each year, bare soil had the highest LST followed by built-up area, vegetation, and water bodies. The results also show that the average temperature for all the classes increased between 1990 and 2014. However, while the average temperature for water body increased slightly by 1.6 °C, the average temperature for bare soil, built-up area, and vegetation increased by an average of 7.5 °C. When we examined the changes in the decadal average temperature per class, significant increases (by 7 °C) were seen between 1990 and 2002 for bare soil and built-up area. The rate of increase reduced to 0.7 °C for these classes between 2002 and 2014. For vegetation class, the rates of increase were 3.14 °C (between 1990 and 2002) and 4.16 °C (between 2002 and 2014).

Table 8. Average LSTs in 1990, 2002, and 2014 for different land cover classes.

Land Cover Class	1990	2002	2014
Bare Soil	37.62	44.41	45.09
Built-Up Area	36.42	43.42	44.12
Vegetation	35.71	38.85	43.01
Water Body	29.04	30.69	30.64

The spatial distributions of the temperatures for 1990, 2002, and 2014 are given in Figure 3, while the relationship between temperature and areal coverage is provided in Table 9. In 1990, the entire study area had LSTs less than 40 °C, with the majority (87.07%) of the land cover having LSTs between 36 °C and 40 °C. In 2002, 77% of the land cover had LSTs between 41 °C and 50 °C. However, the percentage of LSTs between 41 °C and 50 °C increased to 91.26% in 2014, suggesting the study area's LSTs increased between 1990 and 2014, although it increased more in the last decade.
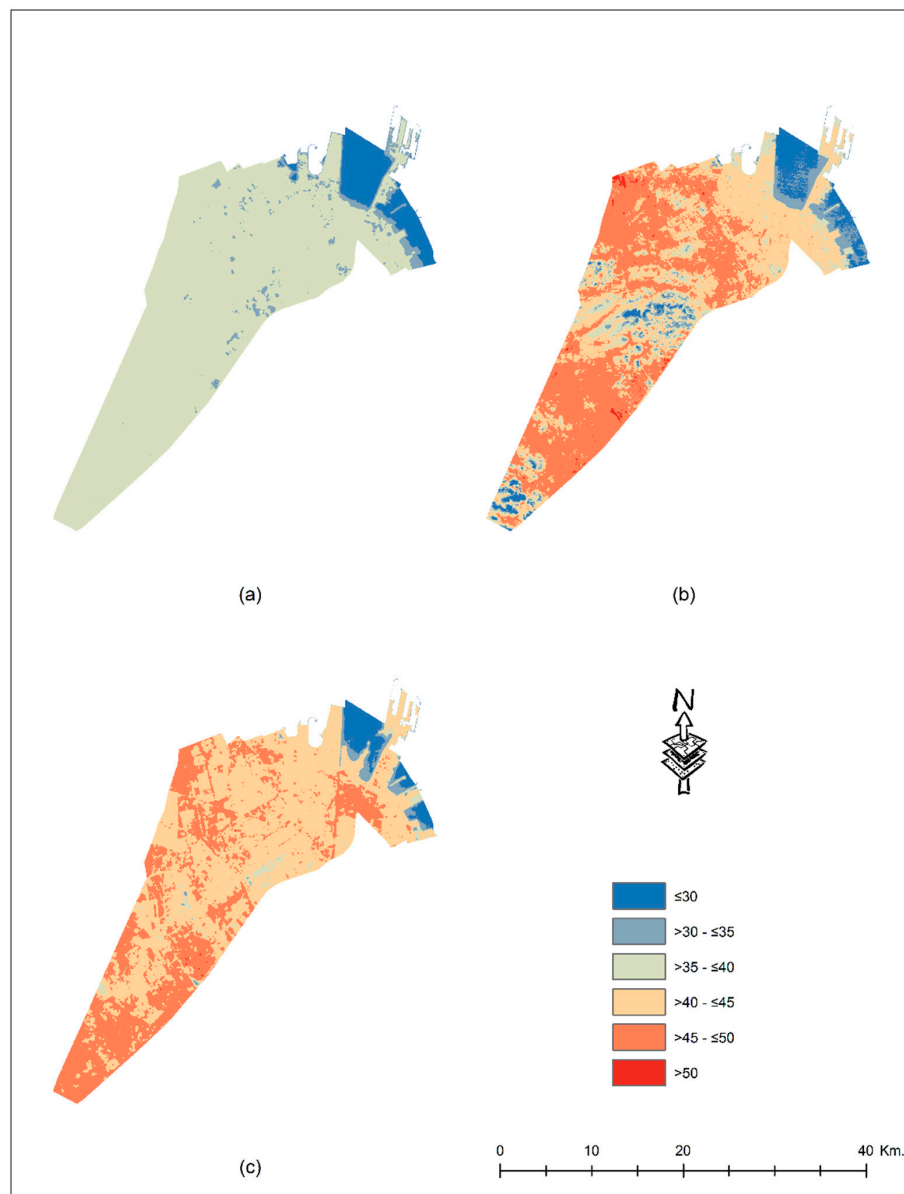

Figure 3. LST distributions for (**a**) 1990, (**b**) 2002, and (**c**) 2014.

**Table 9.** Distribution of areal coverage among different LST ranges for 1990, 2002, 2014, and 2026.

Ranges of LST (°C)	Areal Coverage (%)			
	1990	**2002**	**2014**	**2026**
≤30	7.86	6.14	3.81	0
31 to 35	5.07	6.44	2.3	0.29
36 to 40	87.07	9.9	2.58	1.38
41 to 45	0	36.11	58.69	2.35
46 to 50	0	40.9	32.57	35.06
>50	0	0.51	0.05	60.92

4.3. Modeling of LULC and LST for 2026

Figure 4 shows the simulated LULC for the year 2026 and Table 10 provides their areal statistics. The modeled LULC shows that 35,986 ha (55% of the study area) will change to built-up area, an increase of almost 27.3% from 2014. This increase will mostly occur in the city's northern and southeastern parts. Vegetation will also increase in the city from 1041 ha in 2014 to 3240 ha in 2026 (a gain of 211%) in central northern parts of Dammam and along the northern coastline. This increase in built-up area and vegetation will reduce the amount of bare soil by 8306 ha (a net loss of almost 26%) and water bodies by 1612 ha (loss of roughly 42.5%) from 2014 to 2026. Water bodies will be mostly lost due to new construction of residential and commercial zones along the eastern seashores of the city.
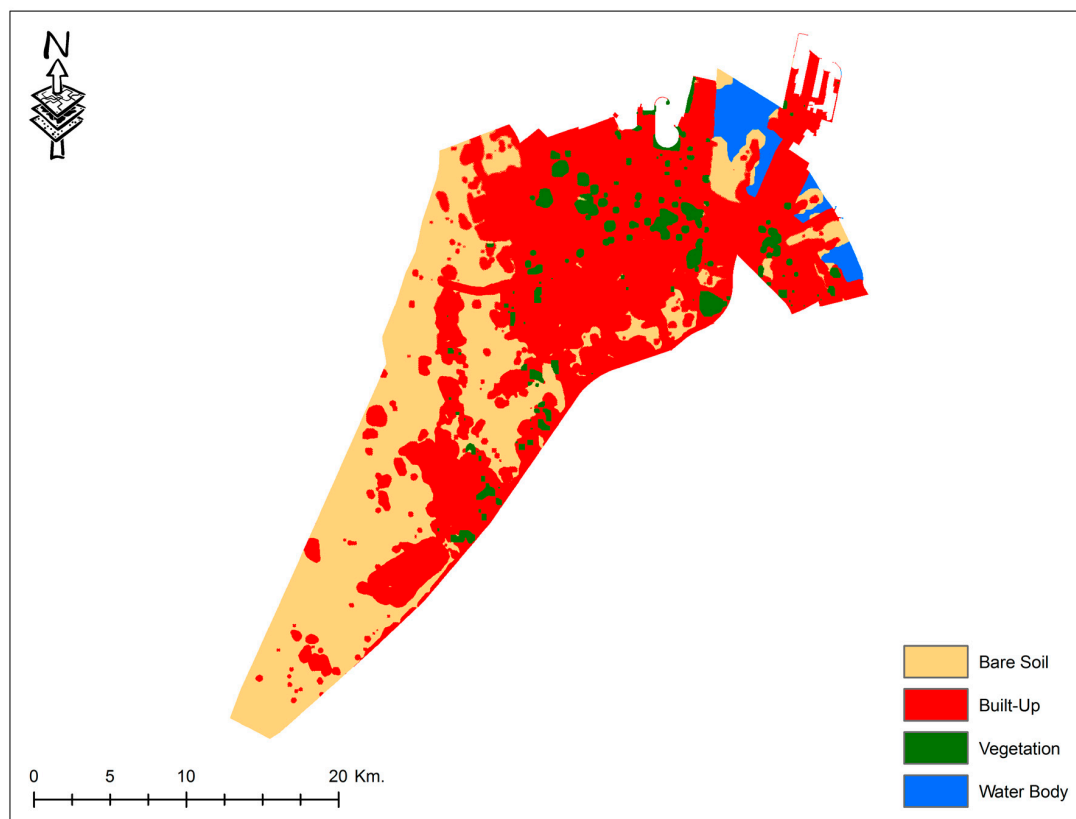
Figure 4. Modeled land use and land cover (LULC) for Dammam for 2026.

The spatial distribution of the modeled 2026 LST is provided in Figure 5 and the areal percentage statistics by LST range is shown in the last column of Table 9. Compared to the LST ranges of 1990, 2002, and 2014, most of the land coverage (98%) is predicted to have LSTs over 41 °C in 2026. The average LSTs for built-up area are forecasted to be 46 °C.
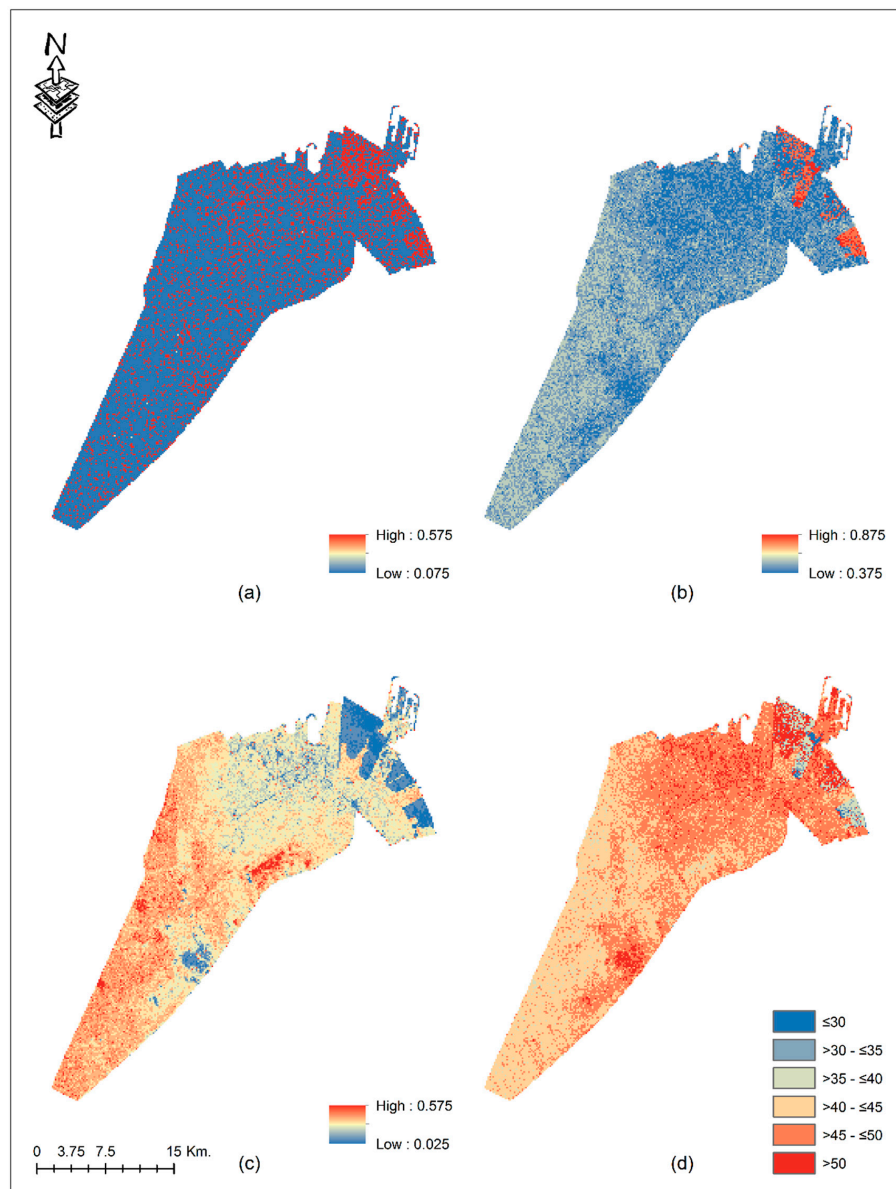
Figure 5. Distribution of the indices ((**a**) NDBI; (**b**) MNDWI; and (**c**) NDBsI) used to model the 2026 LST (**d**) for Dammam.

Table 10. Modelled areal statistics (in hectares) of land cover for 2026.

Land Cover Class	Area	%
Bare soil	23,925	36.62
Built-up area	35,986	55.08
Vegetation	3240	4.96
Water body	2182	3.34
Total	65,333	100

5. Discussions

5.1. Changes in LULC and LSTs

This paper first examined the changes in the LULC in the city of Dammam between 1990 and 2014. The city's urban areas expanded by 61% from 1990 to 2002 and 88% between 2002 and 2014.

Such decadal growth is higher than other cities in Saudi Arabia [19,55]. It is also higher than other developing cities in the world, including Kathmandu [13], Tripoli [56], and Dhaka [57]. Rapid population growth and economic prosperity are the primary reasons for such rapid urban growth [58]. Dammam's population increased from 127,844 (1974) to 260,048 (1986), and finally to 918,154 in 2010 [33,59] due to rapid migration of refugees during and after the 1991 Gulf war from neighboring countries of Iraq and Kuwait. The results also show that the vegetation in the study area decreased between 1990 and 2002 and increased between 2002 and 2014. Previous studies have also found similar patterns of decreasing vegetation coverage between the early 1990s and 2000 and an increase from the early 2000s to 2014 in other Saudi cities [55,60]. They suggested that increasing population resulted in vegetation increases in Saudi cities [60].

In tropical and sub-tropical urban environments, the LSTs are dependent upon the LULC, with urban built-up areas having the highest LSTs and significantly contributing to the formation of UHIs [24,28]. However, having a desert climate, the study area's bare soil (mostly sands) had the highest mean LSTs during the day followed by urban built-up areas in the all of the three years considered. The mean LSTs for vegetative areas were lower than urban built-up areas. Similar resulting patterns were also found in other neighboring desert cities of Abu Dhabi and Dubai, suggesting an inversion of UHIs where city centers are generally cooler than the outskirts of the city due to low vegetation coverage and sand being the main reflecting surface [31,61]. In both cities, a reduction of 5 °C (Abu Dhabi) to 12 °C (Dubai) of mean LSTs were due to the presence of green vegetative areas. For our study area, the vegetative areas lowered the mean LSTs by an average of 2 °C. We believe this slight lowering is due to the very low amount of vegetation present in Dammam (only 1042 ha in 2014), indicating that the reduction in LSTs is correlated to the amount of vegetation present in an area.

It was also found in this study that the mean LSTs of 2014 increased by an average of 7.5 °C when compared to the mean LSTs of 1990. Increases of mean LSTs were also found in Dubai and the semi-arid desert city of Santiago, Chile [61,62]. As highlighted by previous studies, the rapid population growth along with the urban expansion could be the contributing factors to such increases in the temperatures [63].

5.2. LULC and LST Modeling for 2026

The land use and land cover of Dammam are expected to change over the next decade, as 27% of the current LULC is modelled to be converted into urban built-up areas. This decadal growth rate is comparable to other cities in the world, including Setubal and Sesimbra (in Protugal with 25%), Asmara (in Eritrea with 25%), and Beijing (with 31%) [64–66]. Such growth will lead to urban sprawl and will have several benefits and consequences. The benefits include development of industrial infrastructures and facilities which can provide employment opportunities for the residents from small cities and rural areas of the kingdom as well as from other neighboring Arab countries and developing countries of South and Southeast Asia (i.e., Pakistan, Bangladesh, Indonesia, and the Philippines). The expansion can also provide better business, educational, and medical facilities for its residents.

The negative impacts are numerous and most often they outweigh the benefits of the urban expansions. With increasing employment opportunities, the population is projected to grow by almost 20% over the next decade (1,057,256 in 2015 to 1,264,227 in 2025) [33]. Due to increasing population and city expansions, travelling distances for the residents are expected to increase, resulting in more fuel consumption and traffic congestions. The high fuel consumptions will result in rising air pollution and cause various health problems for the elderly and children of the city. The cost for providing public utility services is also expected to rise. Urbanization has also been known to cause social disparities among the residents [67]. Finally, the LST of the city is expected to increase as well from the increasing built-up areas.

The LSTs modelled in this study for 2026 show that the majority of the city will have LSTs over 41 °C, with the average LSTs for built-up areas forecasted to be 46 °C. This is significantly higher than the modelled LSTs of cities in the tropical regions of the world [28]. Recently, Pal and

Eltahir [68] simulated the dry and wet-bulb temperatures for Middle Eastern cities between the years 2071–2100 using a regional climate model. Their study shows that by 2100, the regional average wet-bulb temperature will exceed 35 °C several times in the year and the average maximum dry-bulb temperature exceeding 45 °C in the low lying coastal cities of the region (i.e., Abu Dhabi, Dammam/Dhahran, and Dubai) will become the norm in the July, August, and September summer months. The LSTs modelled in this study are 1 °C higher than the dry-bulb temperature estimated by Pal and Eltahir [68]. This is to be expected, since LSTs and air-temperatures are highly correlated and as the air temperature increases, LST values will tend to be higher than the air temperature [69]. Such extreme high temperatures will be dangerous for human health as well as for animal and plant species. Instead of the end of the century as predicted by Pal and Eltahir [68], these results of this study suggest that Dammam city may experience very high temperatures that may be difficult for human inhabitability within the next one to two decades.

6. Conclusions

This study compared three separate Landsat images to evaluate LULC changes over the last two decades in Dammam, the capitol of Saudi Arabia's Eastern Province. It also examined the trends in the LSTs during these periods and their relationships with the four major LULC classes. Finally, based on the changes, this study projected the LULC and the LSTs for the year 2026. Since 1990, the urban area in Dammam has increased, resulting in decreasing bare soil. The results also show that the average LSTs have increased in the last two decades. If such a trend continues, built-up areas along with the LSTs will continue to increase over the next decade. Such increases in built up areas along with their temperatures will have numerous medical, environmental, and social impacts and consequences.

The study results will be beneficial for Dammam's government officials and planners, who can ensure that the city is growing in a restrictive manner by utilizing and comparing this study's maps with the city's future master plan. They can also create rules and regulations and create strategies that can reduce the LSTs in the city. Future studies should examine in detail the consequences and problems faced by the residents of Dammam due to urban expansions and LST increases as well as how to mitigate them. The growth and the distribution of LSTs of other cities in Saudi Arabia should also be examined and modeled to ensure they are growing in a sustainable manner.

Author Contributions: M.T. Rahman wrote Sections 1, 2 and 4–6 and edited the entire manuscript. A.S. Aldosary and M.G. Mortoja formulated the research design and edited the manuscript. M.G. Mortoja wrote Section 3 and collected and processed all the data for the study.

Conflicts of Interest: The authors declare no conflict of interest.

References

1. McKinney, M.L. Urbanization, Biodiversity, and Conservation. *Bioscience* **2002**, *52*, 883. [CrossRef]
2. Uttara, S.; Elliot, S. Impacts of Urbanization on Environment. *Int. J. Res. Eng. Appl. Sci.* **2012**, *2*, 1637–1645.
3. Maimaitiyiming, M.; Ghulam, A.; Tiyip, T.; Pla, F.; Latorre-Carmona, P.; Halik, Ü.; Sawut, M.; Caetano, M. Effects of green space spatial pattern on land surface temperature: Implications for sustainable urban planning and climate change adaptation. *ISPRS J. Photogramm. Remote Sens.* **2014**, *89*, 59–66. [CrossRef]
4. Gaffin, S.R.; Rosenzweig, C.; Khanbilvardi, R.; Parshall, L.; Mahani, S.; Glickman, H.; Goldberg, R.; Blake, R.; Slosberg, R.B.; Hillel, D. Variations in New York city's urban heat island strength over time and space. *Theor. Appl. Climatol.* **2008**, *94*, 1–11. [CrossRef]

5. Wong, N.H.; Jusuf, S.K. GIS-based greenery evaluation on campus master plan. *Landsc. Urban Plan.* **2008**, *84*, 166–182. [CrossRef]

6. Lai, L.W.; Cheng, W.L. Urban heat island and air pollution–an emerging role for hospital respiratory admissions in an urban area. *J. Environ. Health* **2010**, *72*, 32–35. [PubMed]

7. Priyadarsini, R. Urban Heat Island and its Impact on Building Energy Consumption. *Adv. Build. Energy Res.* **2009**, *3*, 261–270. [CrossRef]

8. Rahman, M.T. Detection of Land Use/Land Cover Changes and Urban Sprawl in Al-Khobar, Saudi Arabia: An Analysis of Multi-Temporal Remote Sensing Data. *ISPRS Int. J. Geo-Inf.* **2016**, *5*, 15. [CrossRef]

9. Al-Ahmadi, F.; Hames, A. Comparison of Four Classification Methods to Extract Land Use and Land Cover from Raw Satellite Images for Some Remote Arid Areas, Kingdom of Saudi Arabia. *J. King Abdulaziz Univ. Sci.* **2009**, *20*, 167–191. [CrossRef]

10. Madugundu, R.; Al-Gaadi, K.A.; Patil, V.C.; Tola, E. Detection of Land Use and Land Cover Changes in Dirab Region of Saudi Arabia Using Remotely Sensed Imageries. *Am. J. Environ. Sci.* **2014**, *10*, 8–18. [CrossRef]

11. Al-Hathloul, S.; Rahman, M.A. Dynamism of metropolitan areas: The case of metropolitan Dammam, Saudi Arabia. *J. Gulf Arab. Penins. Stud.* **2003**, *29*, 11–43.

12. Aguilar, A.G.; Ward, P. Globalization, regional development, and mega-city expansion in Latin America: Analyzing Mexico City's peri-urban hinterland. *Cities* **2003**, *20*, 3–21. [CrossRef]

13. Thapa, R.B.; Murayama, Y. Examining Spatiotemporal Urbanization Patterns in Kathmandu Valley, Nepal: Remote Sensing and Spatial Metrics Approaches. *Remote Sens.* **2009**, *1*, 534–556. [CrossRef]

14. Dewan, A.M.; Yamaguchi, Y. Land use and land cover change in Greater Dhaka, Bangladesh: Using remote sensing to promote sustainable urbanization. *Appl. Geogr.* **2009**, *29*, 390–401. [CrossRef]

15. Jamali, N.A.; Rahman, M.T. Utilization of Remote Sensing and GIS to Examine Urban Growth in the City of Riyadh, Saudi Arabia. *J. Adv. Inf. Technol.* **2016**, *7*, 297–301.

16. Rahman, M.T.; Rashed, T. Urban tree damage estimation using airborne laser scanner data and geographic information systems: An example from 2007 Oklahoma ice storm. *Urban For. Urban Green.* **2015**, *14*, 562–572. [CrossRef]

17. Alwashe, M.A.; Bokhari, A.Y. Monitoring vegetation changes in Al Madinah, Saudi Arabia, using Thematic Mapper data. *Int. J. Remote Sens.* **1993**, *14*, 191–197. [CrossRef]

18. Al-Rowili, M.S.; Fadda, E.H.; Vaughan, R.A. A Comparison of Data Fusion and Unsupervised Classification for Change Detection in Jeddah, Saudi Arabia. In Proceedings of the 22nd Symposium of the European Association of Remote Sensing Laboratories, Prague, Czech Republic, 4–6 June 2002.

19. Aljoufie, M.; Zuidgeest, M.; Brussel, M.; Maarseveen, M.V. Spatial–temporal analysis of urban growth and transportation in Jeddah City, Saudi Arabia. *Cities* **2013**, *31*, 57–68. [CrossRef]

20. Al-Harbi, K.M. Monitoring of agricultural area trend in Tabuk region—Saudi Arabia using Landsat TM and SPOT data. *Egypt. J. Remote Sens. Sp. Sci.* **2010**, *13*, 37–42. [CrossRef]

21. Al-Gaadi, K.A.; Samdani, M.S.; Patil, V.C. Assessment of Temporal Land Cover Changes in Saudi Arabia Using Remotely Sensed Data Precision Agriculture Research Chair, College of Food and Agriculture Sciences. *Middle-East J. Sci. Res.* **2011**, *9*, 711–717.

22. Rao, P.K. Remote sensing of urban "heat islands" from an environmental satellite. *Bull. Am. Meteorol. Soc.* **1972**, *53*, 647–648.

23. Yuan, F.; Bauer, M.E. Comparison of impervious surface area and normalized difference vegetation index as indicators of surface urban heat island effects in Landsat imagery. *Remote Sens. Environ.* **2007**, *106*, 375–386. [CrossRef]

24. Xiao, R.B.; Weng, Q.H.; Ouyang, Z.Y.; Li, W.F.; Schienke, E.W.; Zhang, Z.M. Land surface temperature variation and major factors in Beijing, China. *Photogramm. Eng. Remote Sens.* **2008**, *74*, 451–461. [CrossRef]

25. Li, X.; Zhou, W.; Ouyang, Z.; Xu, W.; Zheng, H. Spatial pattern of greenspace affects land surface temperature: Evidence from the heavily urbanized Beijing metropolitan area, China. *Landsc. Ecol.* **2012**, *27*, 887–898. [CrossRef]

26. Dousset, B.; Gourmelon, F. Satellite multi-sensor data analysis of urban surface temperatures and landcover. *J. Photogramm. Remote Sens.* **2003**, *58*, 43–54. [CrossRef]

27. Chaudhuri, G.; Mishra, N.B. Spatio-temporal dynamics of land cover and land surface temperature in Ganges-Brahmaputra delta: A comparative analysis between India and Bangladesh. *Appl. Geogr.* **2016**, *68*, 68–83. [CrossRef]

28. Ahmed, B.; Kamruzzaman, M.; Zhu, X.; Rahman, M.S.; Choi, K. Simulating Land Cover Changes and Their Impacts on Land Surface Temperature in Dhaka, Bangladesh. *Remote Sens.* **2013**, *5*, 5969–5998. [CrossRef]

29. El Abidine, E.M.Z.; Mohieldeen, Y.E.; Mohamed, A.A.; Modawi, O.; AL-Sulaiti, M.H. Heat wave hazard modelling: Qatar case study. *QScience Connect* **2014**. [CrossRef]

30. Rasul, A.; Balzter, H.; Smith, C. Spatial variation of the daytime Surface Urban Cool Island during the dry season in Erbil, Iraqi Kurdistan, from Landsat 8. *Urban Clim.* **2015**, *14*, 176–186. [CrossRef]

31. Lazzarini, M.; Marpu, P.R.; Ghedira, H. Temperature-land cover interactions: The inversion of urban heat island phenomenon in desert city areas. *Remote Sens. Environ.* **2013**, *130*, 136–152. [CrossRef]

32. Radhi, H.; Sharples, S. Quantifying the domestic electricity consumption for air-conditioning due to urban heat islands in hot arid regions. *Appl. Energy* **2013**, *112*, 371–380. [CrossRef]

33. General Authority for Statistics Population Statistics. Available online: http://www.stats.gov.sa/en/ (accessed on 15 October 2014).

34. WeatherSpark Historical Weather for 2014 in Dammam, Saudi Arabia. Available online: https://weatherspark.com/history/32759/2014/Dammam-Eastern-Province-Saudi-Arabia (accessed on 1 January 2015).

35. NASA Landsat 4–7 Thermal Data to be Resampled to 30 Meters. Available online: https://landsat.gsfc.nasa.gov/landsat-4--7-thermal-data-to-be-resampled-to-30-meters/ (accessed on 30 April 2017).

36. Rozenstein, O.; Karnieli, A. Comparison of methods for land-use classification incorporating remote sensing and GIS inputs. *Appl. Geogr.* **2011**, *31*, 533–544. [CrossRef]

37. Rozenstein, O.; Qin, Z.; Derimian, Y.; Karnieli, A. Derivation of land surface temperature for landsat-8 TIRS using a split window algorithm. *Sensors (Switzerland)* **2014**, *14*, 5768–5780. [CrossRef] [PubMed]

38. Coll, C.; Galve, J.M.; Sánchez, J.M.; Caselles, V. Validation of Landsat-7/ETM+ Thermal-Band Calibration and Atmospheric Correction With Ground-Based Measurements. *IEEE Trans. Geosci. Remote Sens.* **2010**, *48*, 547–555. [CrossRef]

39. Ma, Y.; Kuang, Y.; Huang, N. Coupling urbanization analyses for studying urban thermal environment and its interplay with biophysical parameters based on TM/ETM+ imagery. *Int. J. Appl. Earth Obs. Geoinf.* **2010**, *12*, 110–118. [CrossRef]

40. Wukelic, G.E.; Gibbons, D.E.; Martucci, H.P.; Foote, H.P. Radiometric calibration of Landsat Thematic Mapper thermal band. *Remote Sens. Environ.* **1989**, *28*, 339–347. [CrossRef]

41. Butler, K. Deriving Temperature from Landsat 8 Thermal Bands (TIRS). Available online: http://blogs.esri.com/esri/arcgis/2014/01/06/deriving-temperature-from-landsat-8-thermal-bands-tirs/ (accessed on 3 January 2015).

42. Almutairi, M.K. Derivation of Urban Heat Island for Landsat-8 TIRS Riyadh City (KSA). *J. Geosci. Environ. Prot.* **2015**, *3*, 18–23. [CrossRef]

43. Triantakonstantis, D.; Mountrakis, G. Urban Growth Prediction: A Review of Computational Models and Human Perceptions. *J. Geogr. Inf. Syst.* **2012**, *4*, 555–587. [CrossRef]

44. Guan, D.G.; Li, H.F.; Inohae, T.; Su, W.; Nagaie, T.; Hokao, K. Modeling urban land use change by the integration of cellular automaton and Markov model. *Ecol. Modell.* **2011**, *222*, 3761–3772. [CrossRef]

45. Moghadam, H.S.; Helbich, M. Spatiotemporal urbanization processes in the megacity of Mumbai, India: A Markov chains-cellular automata urban growth model. *Appl. Geogr.* **2013**, *40*, 140–149. [CrossRef]

46. Gong, W.; Li, Y.; Fan, W.; Stott, P. Analysis and simulation of land use spatial pattern in Harbin prefecture based on trajectories and cellular automata-Markov modelling. *Int. J. Appl. Earth Obs. Geoinf.* **2015**, *34*, 207–216. [CrossRef]

47. Halmy, M.W.A.; Gessler, P.E.; Hicke, J.A.; Salem, B.B. Land use/land cover change detection and prediction in the north-western coastal desert of Egypt using Markov-CA. *Appl. Geogr.* **2015**, *63*, 101–112. [CrossRef]

48. Roy, H.G.; Fox, D.M.; Emsellem, K. Predicting Land Cover Change in a Mediterranean Catchment at Different Time Scales. In Proceedings of the 14th International Conference on Computational Science and Its Applications (ICCSA 2014), Guimarães, Portugal, 30 June–3 July 2014; Murgante, B., Misra, S., Rocha, A.M.A.C., Torre, C., Rocha, J.G., Falcao, M.I., Taniar, D., Apduhan, B.O., Gervasi, O., Eds.; Springer International: Cham, Switzerland, 2014.; Volume 8582, pp. 315–330.

49. Visser, H.; Najs, T.D. The Map Comparison Kit. *Environ. Model. Softw.* **2006**, *21*, 346–358. [CrossRef]

50. Chen, X.-L.; Zhao, H.-M.; Li, P.-X.; Yin, Z.-Y. Remote sensing image-based analysis of the relationship between urban heat island and land use/cover changes. *Remote Sens. Environ.* **2006**, *104*, 133–146. [CrossRef]

51.	Huete, A.R. A soil-adjusted vegetation index (SAVI). *Remote Sens. Environ.* **1988**, *25*, 295–309. [CrossRef]

52.	McFeeters, S.K. The use of the Normalized Difference Water Index (NDWI) in the delineation of open water features. *Int. J. Remote Sens.* **1996**, *17*, 1425–1432. [CrossRef]

53.	Xu, H. A Study on Information Extraction of Water Body with the Modified Normalized Difference Water Index (MNDWI). *J. Remote Sens.* **2005**, *9*, 511–517.

54.	Zha, Y.; Gao, J.; Ni, S. Use of normalized difference built-up index in automatically mapping urban areas from TM imagery. *Int. J. Remote Sens.* **2003**, *24*, 583–594. [CrossRef]

55.	Alqurashi, A.F.; Kumar, L. Land Use and Land Cover Change Detection in the Saudi Arabian Desert Cities of Makkah and Al-Taif Using Satellite Data. *Adv. Remote Sens.* **2014**, *3*, 106–119. [CrossRef]

56.	Al-sharif, A.A.A.; Pradhan, B.; Shafri, H.Z.M.; Mansor, S. Spatio-temporal analysis of urban and population growths in tripoli using remotely sensed data and GIS. *Indian J. Sci. Technol.* **2013**, *6*, 5134–5142.

57.	Corner, R.J.; Dewan, A.M.; Chakma, S. Monitoring and Prediction of Land-Use and Land-Cover (LULC) Change. In *Dhaka Megacity: Geospatial Perspectives on Urbanisation, Environment and Health*; Dewan, A.M., Corner, R.J., Eds.; Springer: Dordrecht, The Netherlands, 2014; pp. 75–97.

58.	Abou-Korin, A.A. Impacts of Rapid Urbanisation in the Arab World: the Case of Dammam Metropolitan Area, Saudi Arabia. In *5th Int'l Conference and Workshop on Built Environment in Developing Countries (ICBEDC 2011)*; University Sains Malaysia: Pulao Pinang, Malaysia, 2011; pp. 1–25.

59.	Al-Hathloul, S.; Mughal, M.A. Urban growth management-the Saudi experience. *Habitat Int.* **2004**, *28*, 609–623. [CrossRef]

60.	Aina, Y.A.; Merwe, J.H.V.; Alshuwaikhat, H.M. Urban Spatial Growth and Land Use Change in Riyadh: Comparing Spectral Angle Mapping and Band Ratioing Techniques. In Proceedings of the Academic Track of the 2008 Free and Open Source Software for Geospatial (FOSS4G) Conference, Incorporating the GISSA 2008 Conference, Cape Town, South Africa, 29 September–4 October 2008; pp. 51–57.

61.	Abdi, A. Using Landsat ETM+ to Assess Land Cover and Land Surface Temperature Change in Dubai between 1999 and 2009. Available online: http://www.hakimabdi.com/20120729/using-landsat-etm-to-assess-land-cover-and-land-surface-temperature-change-in-dubai-between-1999-and-2009/ (accessed on 3 March 2016).

62.	Peña, M.A. Examination of the Land Surface Temperature Response for Santiago, Chile. *Photogramm. Eng. Remote Sens.* **2009**, *75*, 1191–1200. [CrossRef]

63.	Brazel, A.; Selover, N.; Vose, R.; Heisler, G. The tale of two climates—Baltimore and Phoenix urban LTER sites. *Clim. Res.* **2000**, *15*, 123–135. [CrossRef]

64.	Tewolde, M.G.; Cabral, P. Urban Sprawl Analysis and Modeling in Asmara, Eritrea. *Remote Sens.* **2011**, *3*, 2148–2165. [CrossRef]

65.	Araya, Y.H.; Cabral, P. Analysis and Modeling of Urban Land Cover Change in Setúbal and Sesimbra, Portugal. *Remote Sens.* **2010**, *2*, 1549–1563. [CrossRef]

66.	Han, H.; Yang, C.; Song, J. Scenario Simulation and the Prediction of Land Use and Land Cover Change in Beijing, China. *Sustainability* **2015**, *7*, 4260–4279. [CrossRef]

67.	Bhatta, B. Causes and Consequences of Urban Growth and Sprawl. In *Analysis of Urban Growth and Sprawl from Remote Sensing Data*; Advances in Geographic Information Science; Springer: Berlin/Heidelberg, Germany, 2010; pp. 17–36.

68.	Pal, J.S.; Eltahir, E.A.B. Future temperature in southwest Asia projected to exceed a threshold for human adaptability. *Nat. Clim. Chang.* **2016**, *6*, 197–200. [CrossRef]

69.	Li, Z.; Guo, X.; Dixon, P.; He, Y. Applicability of Land Surface Temperature (LST) estimates from AVHRR satellite image composites in northern Canada. *Prairie Perspect.* **2008**, *11*, 119–130.